IUST
Iran University of Science and Technology

Iranian Journal of Electrical and Electronic Engineering

Journal Homepage: ijeee.iust.ac.ir

Research Paper

# Feasibility Study of Echocardiographic Images Segmentation Based on Sparse Representation

S. Fouladifard*, H. Behnam*(C.A.), P. Gifani**, and M. Shojaeifard***

**Abstract:** A semi-automatic method for the segmentation of the Left Ventricle in echocardiography images is presented. The manual segmentation of the left ventricle in all image sequences takes a lot of time. The proposed method is based on sparse representation and the design of overcomplete dictionaries based on prior knowledge of the intensity variation time curves (IVTC). We used the sparse recovery algorithm of orthogonal matching pursuit (OMP) to find the sparse coefficients of the IVTC signals. We obtained the histogram of non-zero sparse coefficients for all images. The binary images from successive frames were constructed via thresholding. In addition, we defined one image representing all the frames, dividing all the points of the heart into three groups. One group involved the points located inside the cavities in all frames. The second group included the points that belonged to the tissue in all frames. Points that in some frames are located inside the cavities and in some other frames are located inside the tissue. The results on 2D echocardiographic images acquired from both healthy and patient subjects showed good agreement with manual tracing and took a short time for the contour, including the whole left ventricle. According to the cardiology specialist, the value of ejection fraction is correctly calculated, and the error percentages were 0.83 and 2.33 for two healthy data samples. The proposed method can be applied to 3D echocardiography images to obtain the left ventricular volume. This approach also can be used for other types of medical images.

**Keywords:** Dictionary Design, Echocardiography, Intensity Variation Time Curves (IVTC) Signal, Sparse Representation, Temporal Super-Resolution.

## 1 Introduction

THE leading cause of mortality globally is cardiovascular disease (CVD), taking approximately 17.7 million lives in 2015 and demonstrating an alarming rate of 31% of all deaths. Coronary heart disease and stroke are ranked as the next ones with 7.4 and 6.7 million, respectively. CVD accounts for more than 75% of deaths in low- to middle-income families [1]. The automatic segmentation of the Left Ventricle (LV) of the heart from echocardiography sequences is an essential tool to evaluate the heart's health. The main advantages of echocardiography images over other imaging modalities, such as CT, MRI, and PET, are its low cost, high imaging speed, non-invasiveness, harmlessness, and usage of non-ionizing radiation. The automation of this procedure is agreeable in a clinical setting since it can increase patient throughput and decrease the variability between operator measurements [2]. However, due to speckle noise, non-homogeneities, characteristic artifacts (e.g., the appearance of shadows produced by the dense muscles, edge dropout caused by motion, and attenuation), low signal-to-noise ratio, fast movement during systole phase, negligible contrast exhibited

Iranian Journal of Electrical and Electronic Engineering, 2022.
Paper first received 21 September 2020, revised 17 October 2021, and accepted 18 October 2021.
* The authors are with the Department of Biomedical Engineering, School of Electrical Engineering, Iran University of Science and Technology (IUST), Tehran, Iran.
E-mails: soorin.fooladi@gmail.com and behnam@iust.ac.ir.
** The author is with the Faculty of Medical Sciences and Technology, Islamic Azad University, Science and Research Branch, Tehran, Iran.
E-mail: p.gifani@gmail.com.
*** The author is with the Echocardiography Research Center, Rajaie Cardiovascular Medical and Research Center, Iran University of Medical Sciences, Tehran, Iran.
E-mail: maryam.shojaeifard@yahoo.com.
Corresponding Author: H. Behnam.
https://doi.org/10.22068/IJEEE.18.2.1993

between desired regions, along with the rough and precise automatic segmentation of left ventricle can pose some challenges [3]. A premium has been placed on endocardium motion tracking to measure the left ventricular areas, and also extract the parameters, such as the ejection fraction and cardiac output. The application of these measures is of particular interest in diagnosing and assessing ischemic heart disease [4].

In this study, a semi-automated segmentation of the endocardium in echocardiographic data has been proposed. Segmentation methods can be divided into the following classes: region growth (e.g., fuzzy connectedness [5]), classification (e.g., k-means, thresholding), deformable models with (e.g., snake [6], level set) procedures [7–9], deformable templates [10, 11], active shape models (ASM), active appearance models (AAM) [12, 13], active contour methods [6,14], Markov random fields [15], hybrid and space-frequency methods [16], as well as sparse representation and dictionary learning methods [3,17]. A dynamical projection model derived from sparse representation, and dictionary learning was proposed by Huang et al. to track both endocardial and epicardial contours in the left ventricle in the sequences of echocardiography [3]. A segmentation of the endocardium, characterizing 2-D short-axis echocardiographic images of rats, was proffered by Romero et al. During the classification, the sparse representation of feature vectors was applied over learned dictionaries [17].

This paper presents a new method in the representation of sparse signals and the design of overcomplete dictionaries based on IVTC signals for the segmentation of echocardiographic sequences. The study at hand provides an explanatory account of the materials and methods, such as the IVTC acquisition, the cardiac set description, the sparse reconstruction of temporal signals, and endocardium segmentation methodology in Section 2. In Section 3, the results of the proposed method are presented, and the completion of the proposed process is compared with manually segmented images by an expert cardiologist. The Discussion and conclusion are presented in Section 4.

## 2 Materials and Methods

We presented a new method by sparse representation and overcomplete dictionaries designing according to prior knowledge of the temporal signals (IVTC signals) for the segmentation of cavity and tissue of the left ventricle in echocardiographic sequences. To do the sparse representation and the design of overcomplete dictionaries, we first derived temporal information by extracting IVTC assessed for each pixel. We used the OMP sparse recovery algorithm to find the sparse coefficients of the IVTC signals. Greedy algorithms iteratively approximated the coefficients and the support of the original signal. The method is fast and straightforward for the segmentation of echocardiography sequences.

### 2.1 Clinical Image Dataset

By using a Vivid3 with a 2 MHz probe, the sequence of echocardiography images was obtained. Based on the frame rate, the dataset consisted of four-chamber view sequences of a set of healthy subjects and those with cardiac dysfunction. The frame rate varied between 53 and 60 frames/sec. In this dataset, about one cardiac cycle was recorded for each subject. Fig. 1 shows sample frames. For better presentation, this paper includes video recordings of all frames for the original dataset (videos 1 and 2 show echocardiography images of the first healthy and patient subjects).

The proposed method, in its initial stage, attempts to extract the assessed IVTC (intensity variation time curves) in each individual pixel of consecutive echocardiographic frames. The so-called curves can be characterized by p (x, y, t) corresponding to the pixel in position (x, y), with the frame of time t (t =1, …, T), where T stands for the overall number of frames. An IVTC signal from the fixed coordinate (x, y) of 60 sequential frames is depicted in Fig. 2 [18, 19].

### 2.2 Sparse Representation

Sparse representation is an approach to decode data structures; it also presents an accurate mathematical framework for studying high-dimensional data [20]. As regards the challenge of sparse representation images, in

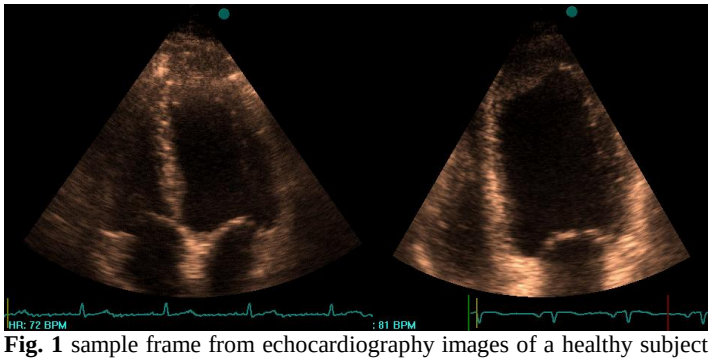


**Fig. 1** sample frame from echocardiography images of a healthy subject (left) and an ischemic patient (right).

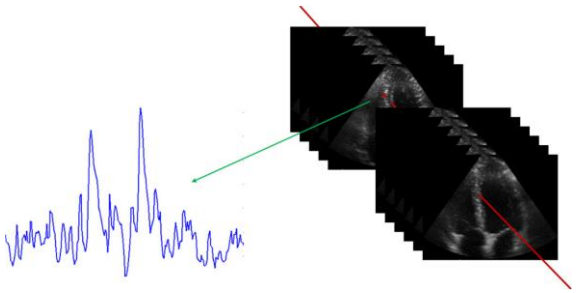

**Fig. 2** Intensity variation time curves of a fixed coordinate (x, y) in all frames [18].

removing noise from images [21], motion detection and data segmentation [22, 23], compression [24], image super-resolution [25], signal classification [26], face recognition [27], texture segmentation and classification [28, 29], and object detection [30]. The focal points of researchers have been three dimensions of sparse representation: pursuit methods to overcome the challenge of optimization, such as matching pursuit (MP) [31], orthogonal matching pursuit (OMP) [32], and basis pursuit [33]; LARS/homotopy methods [34]; dictionary design, e.g., the K-SVD method [21]; and the applications of the sparse representation for different tasks, e.g., denoising, coding, signal separation, and image inpainting [35–39]. The OMP is a greedy algorithm. The basis of this algorithm is identical to the mutual pursuit algorithm; however, the difference between OMP and MP algorithms is that sparse representation coefficients are updated in each step, and the updated coefficient of the previous step is changeable [40].

### 2.3 Dictionary Design

The overcomplete dictionaries can be classified into two different methods. The first one is that of learning an optimum overcomplete dictionary compiled from a specified set of examples, and the other is designating the dictionary using a set of identified mathematic functions (pre-specified functions). If specific signal characteristics are known, a dictionary can, for example, be chosen from the Fourier basis or wavelets. We utilize the OMP algorithm in designing an overcomplete dictionary using pre-specified functions since it is faster and more manageable for evaluating the sparse representation [18]. One of the fundamental issues for representing signals is to choose a dictionary. The primary approach is to present a dictionary that is much more appropriate to all signals in the issues. For example, if the data is echocardiography images, we should look for a suitable dictionary for all parts of the image. We employ sine and cosine functions, as well as four wavelet families based upon the available knowledge of the nature of IVTC signals along with the cyclic behavior of the heart. The wavelet parts are considered in the dictionary because we face minor variations and rapid transitions. One of the critical issues is the selection of adequate main wavelets. To reduce and simplify the complex structure of a dictionary, we use orthogonal wavelets. There are a variety of orthogonal wavelets, such as Symlet, Coiflets, Haar, Daubechies, and discrete Meyer. Four wavelet families are designated among the aforementioned orthogonal wavelets at our disposal, each with the ideal form for the construction of the IVTC: Symlet (sym2), Symlet 4 (sym4), Daubechies 4 (db4), and discrete Meyer (dmey). Therefore, for a signal characterized by the length T, there are T atoms, where T/2 atoms relate to the shifted pulse signals convolution with the scaling functions, and the other T/2 atoms relate to the functions of the wavelet. In total, the number representing each column in the wavelet section in the dictionary indicates 4T for the four wavelet families.

As for the section on sine-cosine, it merely is sufficed to put forth sine and cosine functions:

$$\sin\left(k\times {}^{t}\!/_{T}\right) \text{ and } \cos\left(k\times {}^{t}\!/_{T}\right) \quad k=1,\ldots,{}^{T}\!/_{2} \quad t=1,\ldots,T \tag{1}$$

Hence, we have $T/2$ atoms for the sine section and $T/2$ atoms for the cosine section, respectively. Then, for IVTC signal with length $T$, the overcomplete dictionary features $T$ rows along with $5T$ columns—standing for atoms—, and the relevant sparse coefficient features $5T$ rows:

$$Y\left[T\times 1\right]=D\left[T\times 5T\right]X\left[5T\times 1\right] \tag{2}$$

where $Y$ is an $M\times 1$ signal vector, $X$ represents an $N\times 1$ sparse coefficient vector, and $D$ is an $N\times M$ dictionary matrix. The sparse coefficients $X$ must be computed by a proper sparse recovery algorithm [18].

### 2.4 Sparse Reconstruction of Temporal IVTC

First, sparse representation coefficients of temporal IVTC are computed. Given the sparsity constraint, the set of possible signals size can be significantly downscaled compared to the primary signal space, given the constraint of sparsity. A sample IVTC signal obtained from coordinates of (x, y) for t within the range 1-60 of an actual echocardiography sequence is illustrated In Fig. 3. Applying the sparse representation technique, sampling time and sizable storage space can be decreased by a wide margin.

The optimal local solution in each iteration is sought by the greedy strategy to reach the optimal holistic solution. IVTC signals are reconstructed by the OMP algorithm and designed dictionary.

In the second step, the number of sparse coefficients is examined from various coordinates, which have disparate cardiac textures. These points are located on the cardiac muscle, or the ventricle border, or possibly in the atrial cavity. Although the number of non-zero sparse coefficients for points on the tissue on the ventricle boundary and in the cavity is the same, their amplitudes are varied. The points on the tissue have high amplitudes. The different amplitudes of sparse coefficients can be considered a feature to separate the cavity and the tissue points. Therefore, a low-value threshold is applied to all sparse coefficients to remove small coefficients in the cavity. In this way, it is possible to obtain a varied property to separate points within the cavity and the tissue. A point located on the cavity is shown in Fig. 4(a). Fig. 5(a) shows the sparse coefficients of the IVTC signal of the mentioned point.

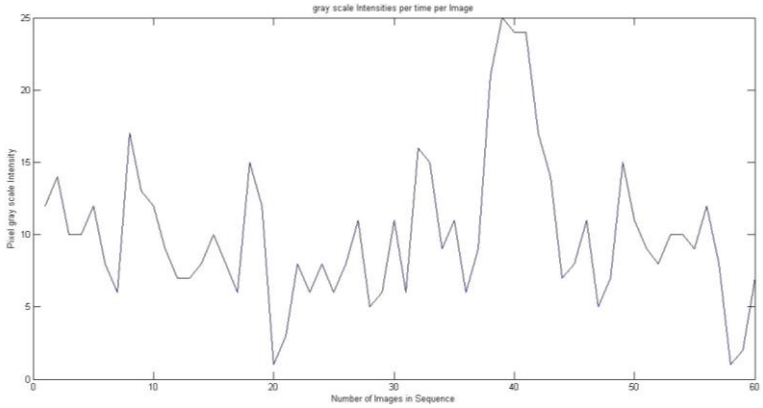


**Fig. 3** A sample IVTC signal for a point on the atrial cavity.

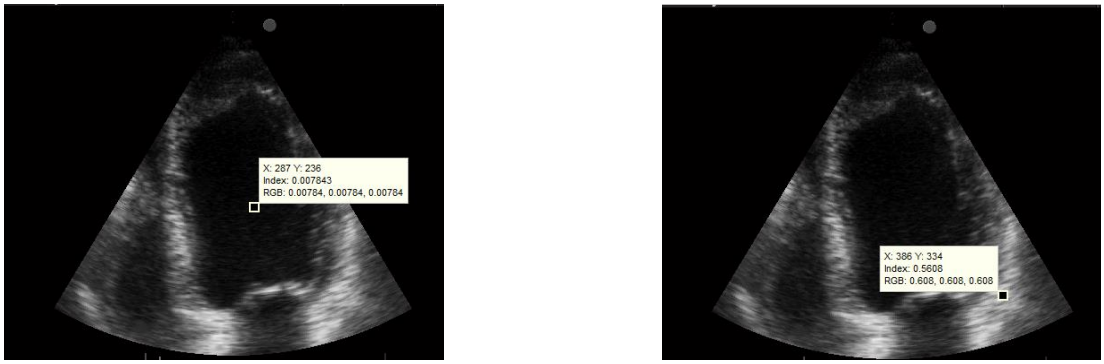


(a) (b)

**Fig. 4** a) A point located in the left ventricular cavity and b) on the cardiac muscle.

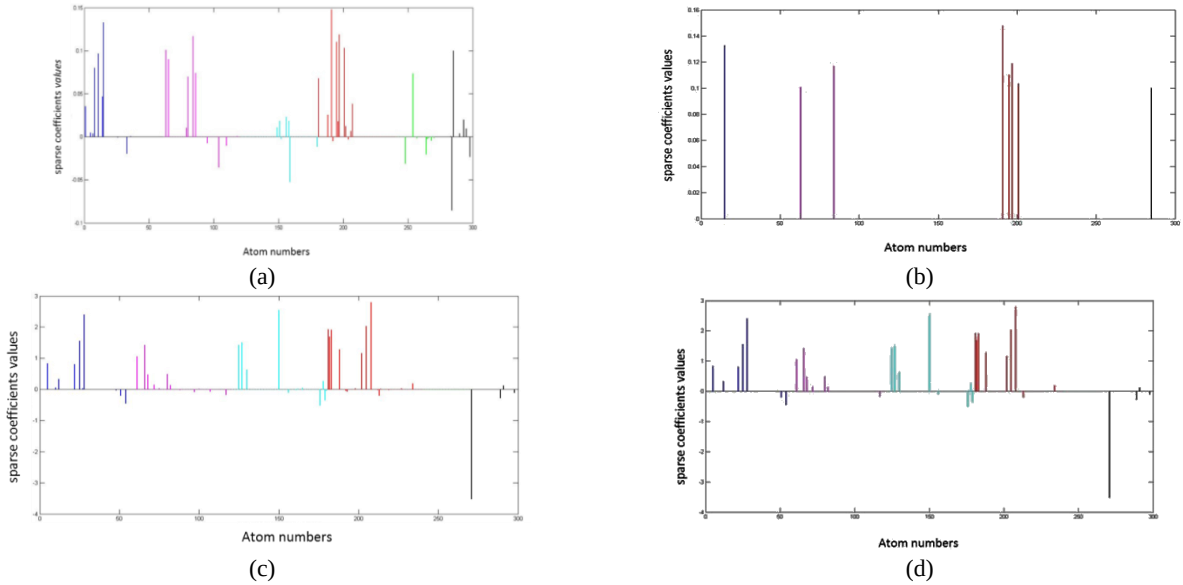


(a) (b)

(c) (d)

**Fig. 5** Sparse coefficients of the IVTC signal of the point shown in Fig.4 that a) was located in the cavity, b) after primary thresholding, c) was located on the cardiac muscle, and d) after primary thresholding of the pixel located on the cardiac muscle.

The X-axis represents the number of dictionary columns (Atom numbers), and the Y-axis shows the values of the sparse coefficients. The maximum absolute value of the sparse coefficients in this example is 0.14. Fig. 5(b) illustrates the pixel coefficients after the initial thresholding; the number of non-zero coefficients is 8. A point located on cardiac muscle is shown in Fig. 4(b). Fig. 5(c) illustrates the sparse coefficients of the just mentioned point; the maximum absolute value of the sparse coefficients is 3.5. Fig. 5(d) shows the pixel coefficients after the initial thresholding; the number of non-zero coefficients is 25. In the same way, the number of non-zero coefficients of a point located on the ventricle border is 15.

### 2.5 Endocardium Segmentation

The number of non-zero sparse coefficients for the points located on the tissue on the ventricle boundary and in the cavity are the same. Therefore, the histogram of the number of pixels with the same number of non-zero sparse coefficients is plotted (Fig. 6(a)). After applying the initial thresholding, the histogram of the number of pixels of non-zero sparse coefficients is drawn. This histogram is used to obtain an acceptable threshold for the segmentation of these points, located on the cardiac muscle, the cavities border, and in the cavities. Fig. 6(c) illustrates the histogram from the healthy subject with the axes X and Y, featuring the number of non-zero coefficients and the number of pixels, respectively. Thresholds are determined based on the histogram diagram, and they are different values for different datasets. Two thresholds are experimentally determined to separate the points located on the muscle and in the cavity. If it is supposed to divide the histogram diagram into five parts (Fig. 6(c)), the first part shows the points located in the cavity, and the last one indicates the points located on the muscle in the successive frames. Thus, the number of remaining sparse coefficients relates to the points where their location is changed by changing the frames. Therefore, all IVTC signals could be divided into three parts based on the sparse representation method.

After the initial thresholding, a figure created by echocardiography sequence is displayed in which the intensities of each pixel rather than their sparse coefficients are considered. After that, the image is called "The number of sparse coefficients". The number of sparse coefficients images of a healthy subject is shown in Fig. 7(a). This image represents all the consecutive frames; the points located on the muscles are indicated by white pixels (one point), the points located in the cavities are shown by black pixels (zero points), and gray points correspond to the pixels, which in some frames are located inside the muscles, and in the other frames contained cavities (e.g., pixels surrounded heart valve or ventricle borders).

Since thresholding is applied to IVTC signals, the points located on the muscles and in cavities (white and black pixels) are fixed on the successive frames. The remaining points are shown with values of their initial brightness intensity. Therefore, another threshold is set on the pixel values over the grayscale range by which the remaining points become binary. In the end, the consecutive images are obtained in binary form. The availability for fast and reliable segmentation is demonstrated by the proposed method results. The block diagram from the proposed method is exhibited in Fig. 8.

## 3 Results

Using a Vivid3 ultrasound imaging system to feature a frame rate of ~60 Hz, 2D echocardiographic sequences are obtained from patient and healthy subjects, each sequence spanning a cardiac cycle. The discriminating sparse representation method is explored in the images of endocardium and echocardiography using experimental analyses.

The number of non-zero sparse coefficients for points located on the tissue on the ventricle boundary and in the cavity are the same; the bar histogram for the

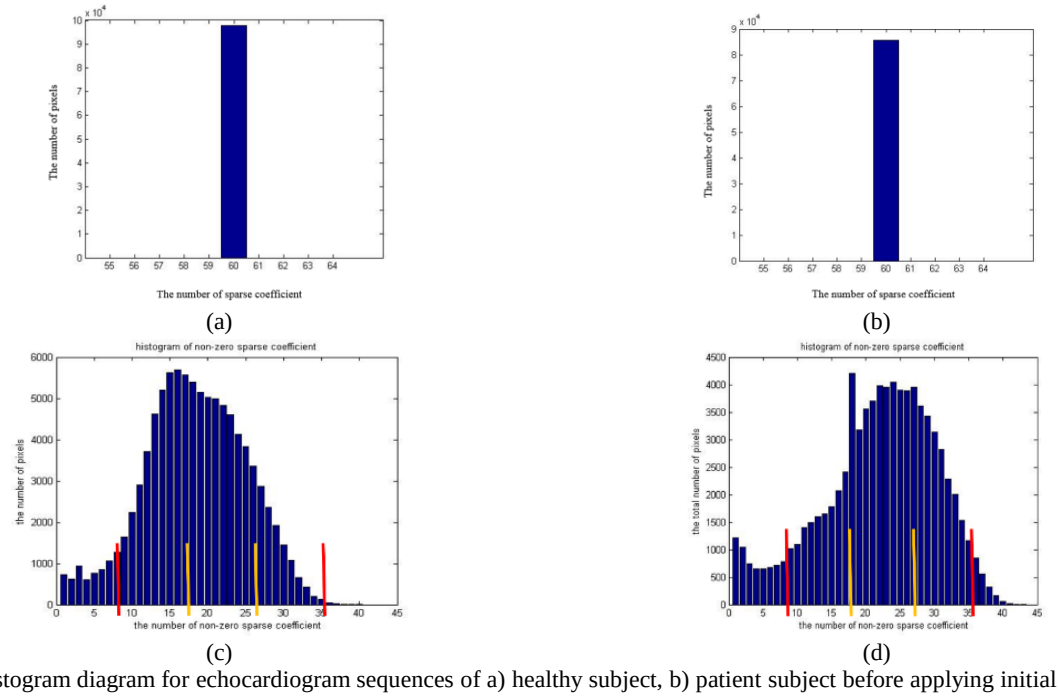


**Fig. 6** Histogram diagram for echocardiogram sequences of a) healthy subject, b) patient subject before applying initial thresholding, c) healthy subject, and d) patient subject after applying initial thresholding.

(a) (b)

**Fig. 7** The number of sparse coefficient's image of a) healthy subject and b) patient subject.

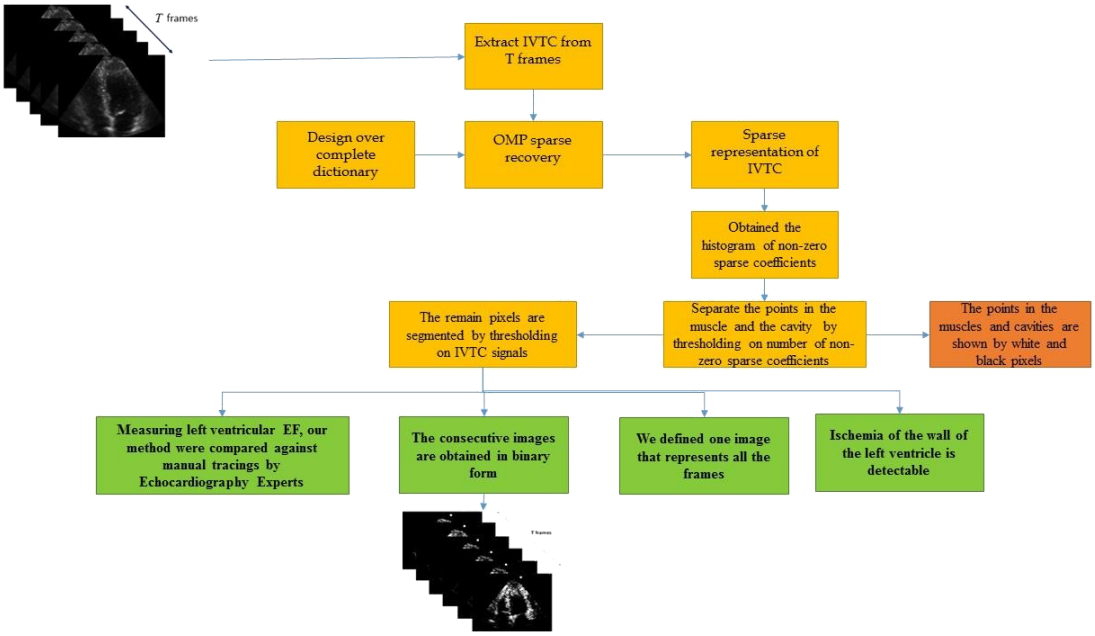


**Fig. 8** Block diagram of the proposed method.

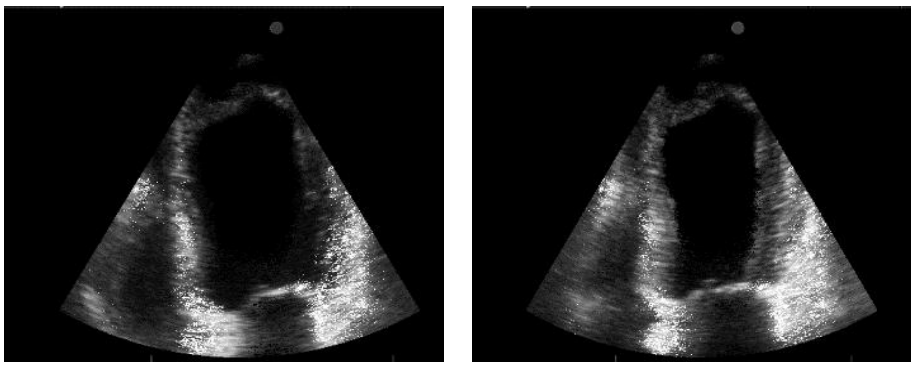

**Fig. 9** Frame 10 of patient images (left) and frame 25 of patient images (right), the points in tissues and cavities (white and black pixels) are fixed on the successive frames.

number of pixels is shown in Fig. 6(b). Therefore, a value of a low threshold is applied to all sparse coefficients for eliminating small coefficients always present in the cavity. The number of non-zero sparse coefficients is different. In this way, it is possible to obtain an additional property to separate points within the cavity and the tissue.

Two thresholds are determined to separate the points located on the muscle from the ones in the cavity. Fig. 6(d) shows the histogram diagram for echocardiogram sequences of a patient (subject) after applying the initial thresholding to divide the histogram diagram into five parts. The first part shows the points in the cavity, and the last part reveals the points inside the muscle.

The number of sparse coefficient images of a patient (subject) is shown in Fig. 7(b), representing all the consecutive frames. Fig. 9 shows frames 10 and 25

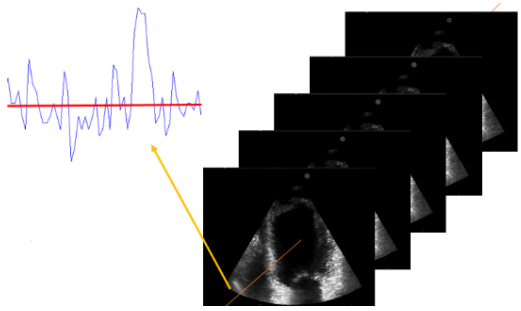

**Fig. 10** Setting another threshold on the gray levels of pixels.

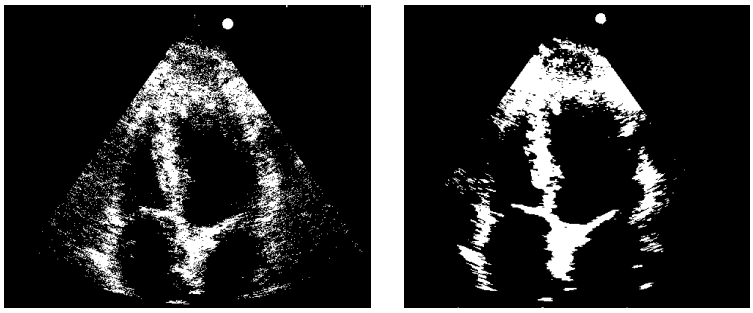

(a) (b)

**Fig. 11** A binary image a) of the proposed method of a healthy subject and b) obtained by setting the threshold to an image of frame 21.

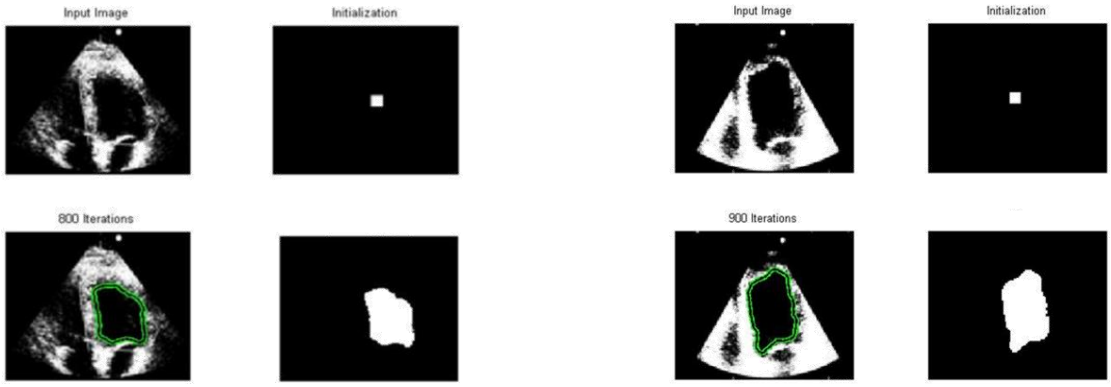


(a) (b)

**Fig. 12** Correct detection of left ventricular borders by active contour without edges method, images related to a a) healthy subject and b) patient subject.

of the patient sample images once the thresholding of the points in muscles and cavities (white and black pixels) are fixed on the successive frames. The remaining points are shown with values of their initial brightness intensity. Afterward, another threshold is set on the pixel values over the grayscale range by which the remaining points become binary (Fig. 10).

Finally, the consecutive images become binary by the proposed method. Fig. 11(a) shows a binary image of the healthy sample subject. Video 3 shows the binary images of the first healthy subject obtained from the following proposed method; also, Video 4 shows the binary images of the first patient subject. According to the comparison results of sparse representation segmentation made by applying a threshold on original clinical data (frame 21), some tissues of the right side of the left ventricle and muscles around the valves are missing (Fig. 11(b)).

### 3.1 Measuring Left Ventricular Ejection Fraction

Left ventricular volumes and ejection fraction are challenging to be assessed by 2D echocardiography; and yet well established as functional parameters. Two-dimensional echocardiography has evolved into a significant and relatively facile method to be used. To evaluate the performance of the proposed method, the surface area of the left ventricular is obtained and an active contour without edges method is used [6]. The end-diastolic and end-systolic frames (when the mitral valve was closed) are considered for computing the ejection fraction.

Firstly, the initialization is performed in the first frame, and then the left ventricle surface area is automatically obtained in the remaining frames. Fig. 12 shows examples of images of patients and healthy subjects. The left ventricle borders are successfully detected. The proposed method is compared with the contour, carefully tracked boundaries of left ventricular manual tracings by an echocardiography expert. Videos 5 and 6 show the left ventricular surface changes in the first healthy and patient subjects obtained from the proposed method.

The proposed method is compared with those of active contour and level set. The active contour method is applied to the initial healthy data. As illustrated in Fig. 13, by changing the control parameters and increasing the iteration number, the contour is stopped in the initial frames and does not cover the left ventricle. Further, an optimal value for left ventricle tracking is achieved using the level set method; the difference with the proposed method is that it took a long time for the contour to cover the whole left ventricle (Fig. 14). Videos 7 and 8 shows the left ventricular surface changes of the left ventricle obtained by the level set in the first and second healthy subject, respectively.

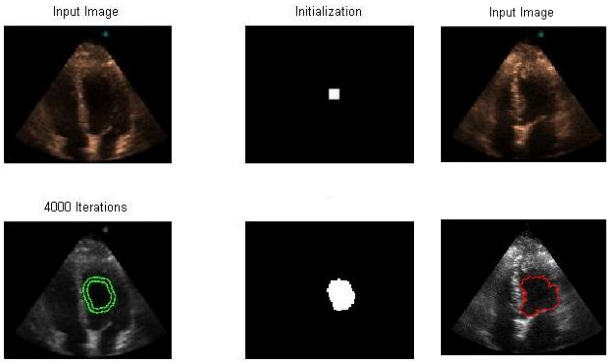


**Fig. 13** The active contour method was applied to the initial healthy subject; the contour was stopped in the initial frames.

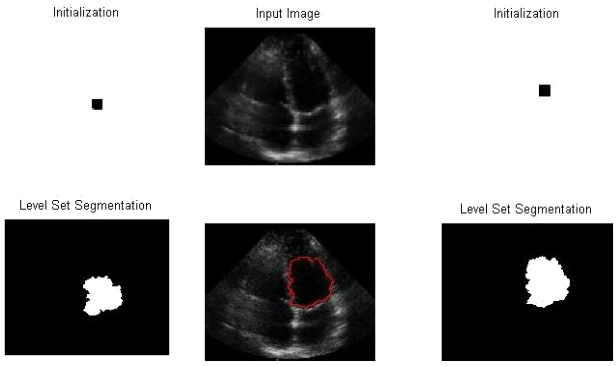


(a) (b)

**Fig. 14** Detection of left ventricular borders by level set method, images related to a a) First healthy subject and b) Second healthy subject.

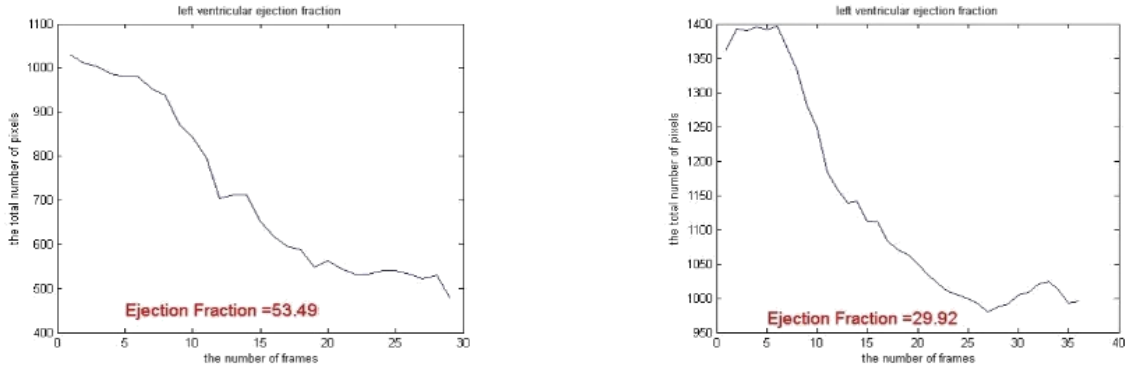


(a) (b)

**Fig. 15** Diagram of left ventricular surface changes in a) healthy subject and b) patient subject.

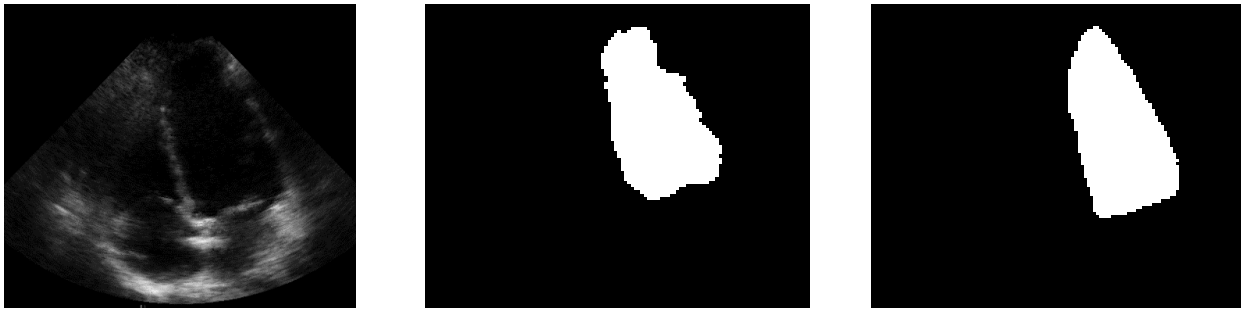

(a) (b) (c)

**Fig. 16** a) Illustrates sample clinical frames of the second healthy subject. The surface of the left ventricle: obtained b) by the proposed method, and c) manual tracing by an expert.

Fig. 15 shows the left ventricular surface changes in patient and healthy subjects. Axes X and Y indicate the number of frames and surface changes of the left ventricle, respectively. Changes in the left ventricular are significantly higher in healthy subjects compared to the patient subjects.

### 3.2 Manual Segmentation and Validation Processes

LV borders can be extracted using a sparse representation method and quantify ejection fraction with good agreement with manual tracing. The 2D frames from ED and ES images are taken, and the left ventricular endocardial border is manually segmented by an expert cardiologist. This manually segmented border is used as ground truth to evaluate the segmentation of the left ventricular obtained using the proposed semi-automatic method. The reference contour and semi-automatically segmented contour are compared using values of ejection fraction described below. The ejection fraction manually obtained by the physician on the left ventricle level is evaluated. There is an insignificant difference between the ejection fraction obtained by the proposed method and the contour of the left ventricle as determined by the physician (manual tracings). Table 1 shows the percentages of the ejection fraction obtained by the proposed method, level set, Otsu, active contour, and the physician for two healthy data samples; the error percentages were 0.83 and 2.33. Fig. 16(a) illustrates sample clinical frames of the second healthy subject.

**Table 1** The percentages of the ejection fraction obtained by the proposed method, level set, Otsu and the physician, and percent error for two healthy subjects.

| Ejection fraction | Manual tracking | Proposed method (Sparse representation + Active contour without edges) / Percent error | level set / Percent error | Otsu + Active contour / Percent error |
|---|---|---|---|---|
| First healthy subject | 53.05 | 53.49 / 0.83 | 51.43 / 3.05 | 45.97 / 13.34 |
| Second healthy subject | 62.88 | 61.41 / 2.33 | 43.32 / 31.1 | 37.21/ 40.82 |

Fig. 16 shows the surface of the left ventricle obtained using the proposed method (right) and manual tracing by an expert (left). Video 9 shows original echocardiography images of the second healthy subject, video 10 shows the left ventricular surface changes in the second healthy subject obtained by the proposed method, and videos 11 and 12 show the left ventricular surface changes in the first and second healthy subjects obtained through the manual tracing. According to the cardiology specialist, the value of ejection fraction is correctly calculated, and the proposed method may be considered novel to obtain ejection fraction.

## 4 Discussion and Conclusion

This paper presents essential aspects of sparse representation and dictionary design in the segmentation of echocardiographic image sequences of humans. The proposed method is based on sparse representation and design of over-complete dictionaries based on prior knowledge of the IVTC temporal signals. Our method achieves the segmentations comparable with manual tracings by experts in echocardiography on healthy and patient data alike. The extrapolations from the ejection fraction calculated from the segmentation results are entirely compatible with manual results. Nevertheless, a limitation arises as there are only two manual tracing results earmarked for healthy data sets. The availability of manual patient results obtained independently from patients may bear a more comprehensive testimony to the method's validity. Furthermore, the technique has only been tested on small datasets. Prospective studies are expected to aim at working out a solution to the existing constraints and promoting its application to further modalities and acquisition settings.

In this article, the OMP greedy algorithm is used due to its simplicity and speed. It is possible to use an optimized algorithm to reconstruct the sparse coefficients. Furthermore, the trained dictionaries can be used instead of designing overcomplete dictionaries using the pre-specified functions. The histogram of non-zero points of sparse coefficients can be compared with more data samples related to healthy individuals or patients. The probability distribution parameters can be obtained with a higher number of datasets. The proposed method can be applied in combination with other techniques of echocardiography images diagnosis to obtain highly accurate computation of the parameters. Besides, the proposed method can be applied to 3D echocardiography images to get the left ventricular volume. Our approach also may be used for other imaging modalities, such as MRI or CT.

## Intellectual Property

The authors confirm that they have given due consideration to the protection of intellectual property associated with this work and that there are no impediments to publication, including the timing of publication, with respect to intellectual property.

## Funding

No funding was received for this work.

## CRediT Authorship Contribution Statement

**S. Fouladifard:** Conceptualization, Methodology, Software, Validation, Formal analysis, Writing - Original draft. **H. Behnam:** Conceptualization, Writing - Review & Editing, Supervision. **P. Gifani:** Data curation, Writing - Review & Editing. **M. Shojaeifard**: Investigation.

## Declaration of Competing Interest

The authors hereby confirm that the submitted manuscript is an original work and has not been published so far, is not under consideration for publication by any other journal and will not be submitted to any other journal until the decision will be made by this journal. All authors have approved the manuscript and agree with its submission to “Iranian Journal of Electrical and Electronic Engineering”.

## References

[1] D. Mozaffarian, A. S. Go, D. K. Arnett, M. J. Blaha, M. Cushman, S. R. Das, S. de Ferranti, J. P. Després, H. J. Fullerton, V. J. Howard, M. D. Huffman, C. R. Isasi, M. C. Jiménez, S. E. Judd, B. M. Kissela, J. H. Lichtman, L. D. Lisabeth, S. Liu, R. H. Mackey, D. J. Magid, D. K. McGuire, E. R. III. Mohler, C. S. Moy, P. Muntner, M. E. Mussolino, K. Nasir, R. W. Neumar, G. Nichol, L. Palaniappan, D. K. Pandey, M. J. Reeves, C. J. Rodriguez, W. Rosamond, P. D. Sorlie, J. Stein, A. Towfighi, T. N. Turan, S. S. Virani, D. Woo, R. W. Yeh, and M. B. Turner, “Heart disease, stroke and research statistics at-a-glance,” *American Heart Association Statistics Committee and Stroke Statistics Subcommittee*. Vol. 64.

[2] G. Carneiro and J. Nascimento, "Robust left ventricle segmentation from ultrasound data using deep neural networks and efficient search methods," in *IEEE International Symposium on Biomedical Imaging: From Nano to Macro*, pp. 1085–1088, 2010.

[3] X. Huang, D. P. Dione, C. B. Compas, X. Papademetris, B. A. Lin, A. Bregasi, A. J. Sinusas, L. H. Staib, and J. S. Duncan, "Contour tracking in echocardiographic sequences via sparse representation and dictionary learning," *Medical Image Analysis*, Vol. 18, pp. 253–271, 2014.

[4] J. A. Noble and D. Boukerroui, "Ultrasound image segmentation: A survey," *IEEE Transactions on Medical Imaging*, Vol. 25, pp. 987–1010, 2006.

[5] J. K. Udupa, "Multiple sclerosis lesion quantification using fuzzy-connectedness principles," *IEEE Transactions on Medical Imaging*, Vol. 16, pp. 598–609, 1997.

[6] M. Kass, A. Witkin, and D. Terzopoulos, "Snakes active contour models," *International Journal of Computer Vision*, Vol. 1, No. 4, pp. 321–331, 1988.

[7] O. Bernard, B. Touil, A. Gelas, R. Prost, and D. Friboulet, "A RBF-based multiphase level set method for segmentation in echocardiography using the statistics of the radiofrequency signal," in *IEEE International Conference on Image Processing (ICIP)*, Vol. 3, pp. III–157, 2007.

[8] N. Lin, W. Yu, and J. S. Duncan, "Combinative multi-scale level set framework for echocardiographic image segmentation," *Medical Image Analysis*, Vol. 7, No. 4, pp. 529–537, 2003.

[9] M. Lynch, O. Ghita, and P. F. Whelan, "Segmentation of the left ventricle of the heart in 3-D+ t MRI data using an optimized nonrigid temporal model," *IEEE Transactions on Medical Imaging*, Vol. 27, No. 2, pp. 195–203, 2008.

[10] J. C. Nascimento and J. S. Marques, "Robust shape tracking with multiple models in ultrasound images," *IEEE Transactions on Image Processing*, Vol. 17, No. 3, pp. 392–406, 2008.

[11] V. Zagrodsky, V. Walimbe, C. R. Castro-Pareja, J. X. Qin, J. M. Song, and R. Shekhar, "Registration-assisted segmentation of real-time 3-D echocardiographic data using deformable models," *IEEE Transactions on Medical Imaging*, Vol. 24, No. 9, pp. 1089–1099, 2005.

[12] T. Cootes, A. Hill, C. Taylor, and J. Haslam, "Use of active shape models for locating structures in medical images," *Image and Vision Computing*, Vol. 12, No. 6, pp. 355–365, 1994.

[13] J. G. Bosch, S. C. Mitchell, B. P. F. Lelieveldt, F. Nijland, O. Kamp, M. Sonka, and J. H. C. Reiber, "Automatic segmentation of echocardiographic sequences by active appearance motion models," *IEEE Transactions on Medical Imaging*, Vol. 21, No. 11, pp. 1374–1383, 2002.

[14] V. Chalana, D. T. Linker, D. R. Haynor, and Y. Kim, "A multiple active contour model for cardiac boundary detection on echocardiographic sequences," *IEEE Transactions on Medical Imaging*, Vol. 15, No. 3, pp. 290–298. 1996.

[15] K. Held, E. R. Kops, B. J. Krause, W. M. Wells, R. Kikinis, and H. W. Müller-Gärtner, "Markov random field segmentation of brain MR images," *IEEE Transactions on Medical Imaging*, Vol. 16, No. 6, pp. 878–886, 1997.

[16] E. D. Angelini, A. F. Laine, S. Takuma, J. W. Holmes, and S. Homma, "LV volume quantification via spatiotemporal analysis of real-time 3-D echocardiography," *IEEE Transactions on Medical Imaging*, Vol. 20, No. 6, pp. 457–469, 2001.

[17] R. Rosas-Romero and H. D. Tagare, "Segmentation of endocardium in ultrasound images based on sparse representation over learned redundant dictionaries," *Engineering Applications of Artificial Intelligence*, Vol. 29, pp. 201–210, 2014.

[18] P. Gifani, H. Behnam, F. Haddadi, Z. A. Sani, and M. Shojaeifard, "Temporal super resolution enhancement of echocardiographic images based on sparse representation," *IEEE Transactions on Ultrasonics, Ferroelectrics, and Frequency Control*, Vol. 63, No. 1, pp. 6–19, 2016.

[19] P. Gifani, H. Behnam, and Z. A. Sani, "Noise reduction of echocardiographic images based on temporal information," *IEEE Transactions on Ultrasonics, Ferroelectrics, and Frequency Control*, Vol. 61, No. 4, pp. 620–630, 2014.

[20] R. G. Baraniuk, E. Candes, M. Elad, and Y. Ma, "Applications of sparse representation and compressive sensing," in *Proceedings of the IEEE*, Vol. 98, No. 6, pp. 906–909, 2010.

[21] M. Aharon, M. Elad, and A. Bruckstein, "K-SVD: An algorithm for designing overcomplete dictionaries for sparse representation," *IEEE Transactions on Signal Processing*, Vol. 54, No. 11, pp. 4311–4322, 2006.

[22] E. Elhamifar and R. Vidal, "Sparse subspace clustering," in *IEEE Conference on Computer Vision and Pattern Recognition*, pp. 2790–2797, Jun. 2009.

[23] S. R. Rao, R. Tron, R. Vidal, and Y. Ma, "Motion segmentation via robust subspace separation in the presence of outlying, incomplete, or corrupted trajectories," in *26th IEEE Conference on Computer Vision and Pattern Recognition (CVPR)*, pp. 1–8, 2008.

[24] M. W. Marcellin, M. J. Gormish, A. Bilgin, and M. P. Boliek, "An overview of JPEG-2000," in *Data Compression Conference (DCC 2000)*, pp. 523–541, Mar. 2000.

[25] J. Yang, J. Wright, T. S. Huang, and Y. Ma, "Image super-resolution via sparse representation," *IEEE Transactions on Image Processing*, Vol. 19, pp. 2861–2873, 2010.

[26] K. Huang and S. Aviyente, "Sparse representation for signal classification," *Advances in Neural Information and Processing Systems 19 (NIPS)*, pp. 609–616, 2007.

[27] J. Wright, A. Y. Yang, A. Ganesh, S. S. Sastry, and Y. Ma, "Robust face recognition via sparse representation," *IEEE Transactions on Pattern Analysis and Machine Intelligence*, Vol. 31, No. 2, pp. 210–227, 2008.

[28] J. Mairal, M. Leordeanu, F. Bach, M. Hebert, and J. Ponce, "Discriminative sparse image models for class-specific edge detection and image interpretation," in *Lecture Notes in Computer Science (Including Subseries Lecture Notes in Artificial Intelligence and Lecture Notes in Bioinformatics)*, pp. 43–56, 2008.

[29] J. Wright, Y. Ma, J. Mairal, G. Sapiro, T. S. Huang, and S. Yan, "Sparse representation for computer vision and pattern recognition," in *Proceedings of the IEEE*, Vol. 98, No. 6, pp. 1031–1044, 2010.

[30] S. Agarwal and D. Roth, "Learning a sparse representation for object detection," *European Conference on Computer Vision*, Springer, Berlin, Heidelberg, pp. 113–127, 2002.

[31] S. G. Mallat and Z. Zhang, "Matching pursuits with time-frequency dictionaries," *IEEE Transactions on Signal Processing*, Vol. 41, No. 12, pp. 3397–3415, 1993.

[32] Y. Pati, "Orthogonal matching pursuit: recursive function approximation with applications to wavelet decomposition," in *IEEE Proceedings of 27th Asilomar Conference on Signals, Systems and Computers*, pp. 40–44, 1993.

[33] S. S. Chen, D. L. Donoho, and M. A. Saunders, "Atomic decomposition by basis pursuit," *SIAM Journal on Scientific Computing*, Vol. 43, No. 1, pp. 129–159, 1998.

[34] I. Drori and D. L. Donoho, "Solution of $l_1$ minimization problems by LARS/homotopy methods," *IEEE International Conference on Acoustics, Speech and Signal Processing* (ICASSP 2006), Vol. 3, pp. III–III, 2006.

[35] M. Elad and M. Aharon, "Image denoising via learned dictionaries and sparse representation," in *Proceedings of the IEEE Computer Society Conference on Computer Vision and Pattern Recognition*, pp. 895–900, 2006.

[36] M. Elad, B. Matalon, and M. Zibulevsky, "Image denoising with shrinkage and redundant representations," in *Proceedings of the IEEE Computer Society Conference on Computer Vision and Pattern Recognition (CVPR'06)*, Vol. 2, pp. 1924–1931, 2006.

[37] B. A. Olshausen, P. Sallee, and M. S. Lewicki, "Learning sparse image codes using a wavelet pyramid architecture," *Advances in Neural Information Processing Systems*, pp. 887–893, 2001.

[38] J. L. Starck, M. Elad, and D. L. Donoho, "Image decomposition via the combination of sparse representations and a variational approach," *IEEE Transactions on Image Processing*, Vol. 14, No. 10, pp. 1570–1582, 2005.

[39] Y. Li, A. Cichocki, and S. I. Amari, "Analysis of sparse representation and blind source separation," *Neural Computation*, Vol. 16, No. 6, pp. 1193–1234, 2004.

[40] G. Kutyniok, "Theory and applications of compressed sensing," *GAMM Mitteilungen*, Vol. 36, No. 1, pp. 79–101, 2013.

**S. Fouladifard** received the B.Sc. degree in Biomedical Engineering from the Sahand University of Technology, Tabriz, Iran, in 2013, the M.Sc. degree from Iran University of Science and Technology, Tehran, Iran, in 2017. Since 2017, she has been working with the Tehran University of Medical and Sciences as a medical equipment expert, her research interests include image processing, signal processing, medical imaging, and deep learning.

**H. Behnam** received the B.Sc. degree in electrical engineering from Iran University of Science and Technology, Tehran, Iran, in 1988, the M.Sc. degree in Medical Engineering from Sharif University of Technology, Tehran, Iran, in 1992, and the Ph.D. degree in Applied Electronics from Tokyo Institute of Technology, Tokyo, Japan, in 1998. Since 1998, he has been a Researcher with Iran Research Organization for Science and Technology, Tehran, Iran and from 2004, he has been a Faculty Member with Iran

University of Science and Technology (IUST), Tehran, Iran. Currently, he is an Associate Professor of Biomedical Engineering with IUST. His research interests include ultrasound in medicine, medical image processing, and medical signal processing.

**P. Gifani** received the B.Sc. degree in Electrical Engineering from Ferdowsi University of Mashhad, Mashhad, Iran, in 2007, the M.Sc. degree and the Ph.D. degree in medical engineering both from Iran University of Science and Technology, Tehran, Iran, in 2010. Currently, she is an Assistant Professor at the Faculty of Medical Sciences and Technology, Islamic Azad University, Science and Research Branch, Tehran, Iran. Her research interests include sparse representation, compressive sensing, medical image processing, and echocardiography.

**M. Shojaeifard** received medical degree at Yazd University of Medical Sciences, Yazd, Iran in 2000. She was Resident of cardiology in Rajaei Cardiovascular Medical and Research center, Iran University, Tehran, Iran in Oct. 2003–Sep. 2007 and completed fellowships in Echocardiography (Sep. 2008–Mar. 2010), at Rajaei Cardiovascular Medical and Research center, Iran University of Medical Sciences. Her research interests are basic and clinical echocardiography. Currently she is an Associate Professor of Cardiology in Echocardiography Department, Shahid Rajaie Cardiovascular Medical and Research Center, Iran University of Medical Sciences, Tehran, Iran.

© 2022 by the authors. Licensee IUST, Tehran, Iran. This article is an open-access article distributed under the terms and conditions of the Creative Commons Attribution-NonCommercial 4.0 International (CC BY-NC 4.0) license (https://creativecommons.org/licenses/by-nc/4.0/).